University of Kent

Kent Academic Repository

Khan, Ferdous Irtiaz, Hossain, Md. Moinul, Lu, Gang and Wang, Lijuan (2026) ***Health monitoring of lithium-ion battery through magnetic field sensing.*** **In: 2026 IEEE International Instrumentation and Measurement Technology Conference (I2MTC). . E-ISBN 979-8-3315-8938-7.**

Downloaded from

https://kar.kent.ac.uk/113429/ The University of Kent's Academic Repository KAR

The version of record is available from

https://doi.org/10.1109/I2MTC66907.2026.11694621

This document version

Author's Accepted Manuscript

DOI for this version

Licence for this version

CC BY (Attribution)

Additional information

For the purpose of open access, the author(s) has applied a Creative Commons Attribution (CC BY) licence to any Author Accepted Manuscript version arising.

Versions of research works

Versions of Record

If this version is the version of record, it is the same as the published version available on the publisher's web site. Cite as the published version.

Author Accepted Manuscripts

If this document is identified as the Author Accepted Manuscript it is the version after peer review but before type setting, copy editing or publisher branding. Cite as Surname, Initial. (Year) 'Title of article'. To be published in ***Title of Journal*** , Volume and issue numbers [peer-reviewed accepted version]. Available at: DOI or URL (Accessed: date).

Enquiries

If you have questions about this document contact ResearchSupport@kent.ac.uk. Please include the URL of the record in KAR. If you believe that your, or a third party's rights have been compromised through this document please see our Take Down policy (available from https://www.kent.ac.uk/guides/kar-the-kent-academic-repository#policies).

Health Monitoring of Lithium-ion Battery through Magnetic Field Sensing

Ferdous Irtiaz Khan*, Md. Moinul Hossain**, Gang Lu*†, Lijuan Wang*
* *School of Engineering, Mathematics and Physics, University of Kent*
Canterbury, Kent CT2 7NT, UK
fk239@kent.ac.uk, *m.hossain@kent.ac.uk, g.lu@kent.ac.uk, L.Wang@kent.ac.uk
† *International Research Centre for Carbon Neutralization,*
Hangzhou International Innovation Institute, Beihang University
Hangzhou, China

***Abstract*—Lithium-ion batteries require reliable non-invasive monitoring techniques to ensure safety, longevity, and optimal performance. While conventional battery management systems rely on voltage, current, and temperature measurements, these parameters provide limited insight into internal mechanical and electrochemical changes associated with ageing and degradation. Although magnetic field (MF) based approaches have been explored conceptually, their experimental validation for lithium-ion batteries remains limited. This paper presents a non-invasive MF sensing framework based on a dual-coil inductive system that monitors changes in the voltage of a secondary coil induced by battery's state dependent magnetic interactions. A systematic experimental methodology is developed and validated across lithium-ion cells of different capacities, discharge rates, and health conditions. Results show that the proposed MF sensing approach provides a smooth, robust, and voltage-normalized response that scales with battery size and degradation state, exhibiting significantly higher effective sensitivity over narrow operating windows compared to mechanical strain sensing. These findings demonstrate that MF sensing can capture bulk internal state changes associated with both state-of-charge and state-of-health, offering a low-cost, compact, and non-invasive alternative for advanced battery monitoring applications.**

***Index Terms*—Magnetic field sensing, Lithium-ion battery, State of charge, State of health**

I. Introduction

The global shift towards sustainable energy solutions has seen a dramatic increase in the use of lithium-ion (Li-ion) batteries across different sectors. Several factors explain their growing popularity: high energy density, efficiency, incentive-based government policy, and affordability [1]. As Li-ion batteries become more popular, there is a need for a robust monitoring system that can operate in real-time, correctly predict the state of charge (SoC) and state of health (SoH), and is affordable for battery's state-dependent conditions. In terms of safety aspects, this is more crucial, as batteries might face catastrophic failures such as thermal ejection or internal short circuits [2].

Traditionally, battery parameters such as voltage, current, temperature, and pressure are measured using invasive sensors. For example, in an electric vehicle, SoC and SoH monitoring are often examined through voltage, current, and temperature data. Although non-invasive sensors are used for the measurement of current, voltage and temperature data require invasive measurement techniques. Invasive measurements often require cell disassembly, capacity fade, complex design, reduced space, and lack of reproducibility. Furthermore, these systems are not ideal for compact and lightweight applications, such as in portable electronics or electric vehicles.

Given the limitations, there is an increasing demand for non-invasive monitoring of Li-ion batteries. Non-invasive techniques can provide critical data without compromising the integrity of the battery. These techniques harness external measurements that can infer the internal state of the lithium-ion battery. They have gained significant attention for their ability to improve battery safety and reliability, which is crucial for high-energy applications [3]. Furthermore, non-invasive techniques reduce the risks of invasive approaches and allow continuous monitoring over extended periods, providing real-time insights into a battery's operational state.

Table I shows a comparison of recently developed sensing techniques for Li-ion battery monitoring. For example, imaging techniques like digital image correlation (DIC) [4] and X-Ray [5] can be used to monitor the SoC and SoH. However, they are expensive, complex, and pose a potential health hazard. Invasive techniques such as Electrochemical Dilatometry (ECD) proposed by Escher et al. can provide both chemical changes and structural deformations [6]. They are not suitable for real-time monitoring due to the complex setup.

Fibre Bragg Grating (FBG) sensors are widely used in Li-ion batteries for measuring both temperature and stress [7]. They are invasive, fragile, and drilling into the battery is often necessary. Gold et al. proposed a non-invasive acoustic sensing technique using an ultrasonic signal and a piezo-transducer [8]. This technique is used to monitor the SoC, SoH and also to determine cracks inside the battery. They are limited by complex signal interpretation and noise. In terms of magnetic field (MF) probing, Khare et al. proposed MF sensing on lead acid batteries and were successful in monitoring the SoH [9]. A lead-acid battery has a different chemistry compared to Li-ion and is less popular in recent times. A simulation-based method was examined by Singh et al., which produced a relation between MF and surface electrolyte interphase (SEI)

TABLE I
RECENT SENSING TECHNIQUES USED FOR LI-ION BATTERY'S HEALTH MONITORING

Sensing Principle	Examples of Sensor	Advantages	Limitations
Imaging	DIC [4], X-Ray [5]	Non-invasive and high accuracy	Expensive, complex and health hazard
Electrochemical	ECD [6]	Monitors chemical and structural changes	Invasive and limited use
Optical	FBG [7]	Gives precise measurement of temperature and strain	Fragile and invasive
Acoustic	Piezoelectric, ultrasonic [8]	Captures internal cracking	Signal integration is complex, susceptible to noise
Magnetic Field (proposed)	Inductive coils	Enhance battery life, non-invasive, simple and cheap	Susceptible to external MF, not tested for real-world applications

but was not tested on real batteries [10]. As a result, there remains a clear lack of experimentally validated MF sensing frameworks for Li-ion batteries that are demonstrated across different cell capacities, operating conditions, and degradation states.

MF offers several performance and diagnostic advantages for Li-ion batteries. For example, they can enhance battery performance by accelerating Lithium-ion diffusion, improving electrode crystal orientation, and reducing ion concentration polarization [11]. Furthermore, the magnetohydrodynamic effect, driven by the Lorentz force, induces electrolyte convection. This leads to a more uniform distribution of lithium ions and can suppress dendrite formation [12]. Thus, if MF can be used for diagnosing Lithium batteries, it has the potential to enhance battery capacity and serve as a monitoring tool. However, despite these advantages, the practical application of MF-based techniques for Li-ion battery monitoring remains limited, with few studies providing systematic experimental validation across different battery sizes, operating conditions, and degradation states.

This paper proposes a novel MF probing technique utilising two inductive coils to address the gap in MF sensing. Its applicability for real-world lithium-ion battery monitoring is evaluated through a systematic experimental framework. The robustness of the proposed method is assessed by examining the MF sensor's root mean square (RMS) voltage response across various battery capacities, discharge rates and comparing it to a force sensor. The results are further evaluated using a deliberately degraded Li-ion cell.

II. METHODOLOGY

A. Magnetic Field Coupling to Li-ion Battery

This study uses a magnetic sensing approach. It's based on the idea that lithium-ion battery electrochemical and structural changes influence the local magnetic environment when the battery acts as a medium for the magnetic field path. Therefore, if a magnetic field is created using a two-coil system that induces an electromotive force from the primary to the secondary coil, the change in the root mean square voltage of the secondary coil can be used to monitor the battery. This configuration enables non-contact probing of the battery by allowing changes in internal current distribution and magnetic interactions to modulate the coupling between the excitation and sensing coils. As lithium intercalates into and deintercalates from the electrode materials during charging and discharging, the composition and phase of active materials change, leading to variations in magnetic susceptibility (χ) and permeability (μ). The local MF generated by the excitation coil can be approximated as:

$$B(t) = \mu_0 \mu_r(t).H(t) \tag{1}$$

where μ_0 is the permeability of free space, and $\mu_r(t)$ is the relative permeability of the battery, which varies with lithium redistribution and electrode lattice strain. $H(t)$ is the MF strength.

The induced voltage in the receiving coil is proportional to the rate of change of magnetic flux Φ:

$$V_{RMS} \propto \frac{d\phi}{dt} = \frac{d}{dt}\int_S B(t).dA \tag{2}$$

Thus, variations in $\mu_r(t)$ directly influence $B(t)$, altering the RMS output. This can be correlated to the charge and discharge transitions or SoC tracking.

Battery aging leads to phenomena such as SEI layer thickening, lithium plating, loss of active material, and internal microstructural damage and these impact electrical conductivity and magnetic losses. The effects can be shown by complex magnetic permeability:

$$\mu = \mu' - j\mu'' \tag{3}$$

where μ' is the magnetic energy storage and μ'' is the loss due to resistive behavior.

As a result, aged or damaged batteries will exhibit greater magnetic damping and altered field propagation, leading to measurable changes in signal amplitude. A comparative reduction or shift in RMS across repeated cycles can thus be used as a proxy for capacity fade or internal deterioration.

B. Measurement Framework

The measurement framework is designed to test MF sensing for monitoring internal mechanical and electrochemical changes in lithium-ion batteries under varying conditions. The full methodology is illustrated in Fig. 1.

The measurement framework starts by optimising the placement and orientation of the MF sensor relative to the excitation

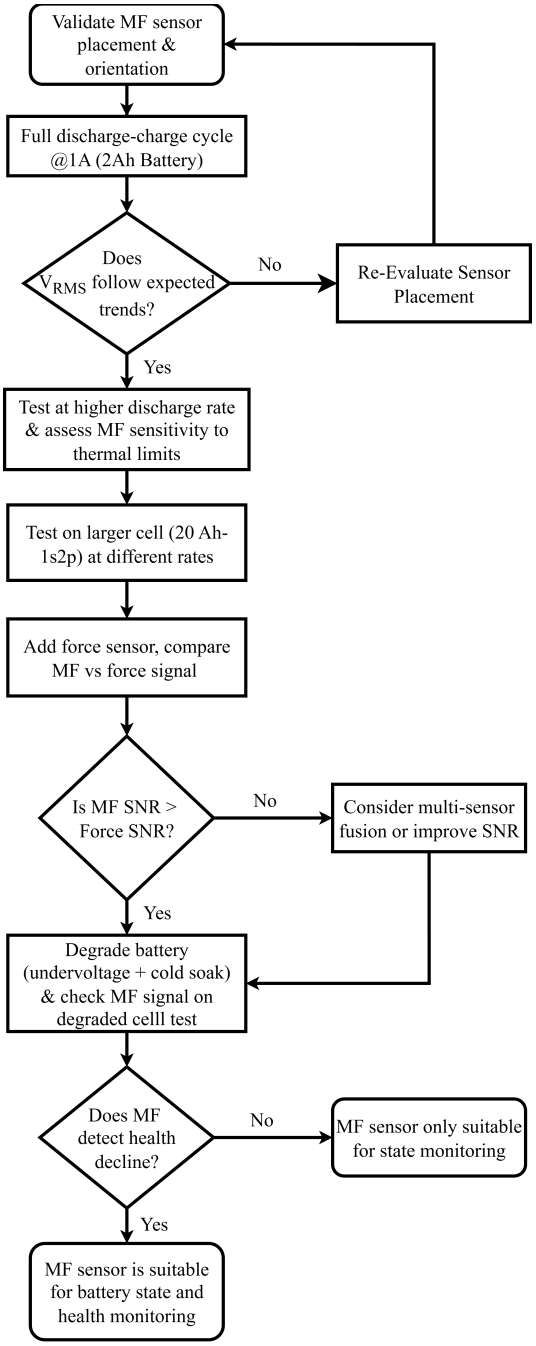


Fig. 1. Flowchart of the proposed measurement framework for evaluating the MF sensor's applicability in battery health monitoring.

coil and battery body. Once the sensor geometry was fixed based on signal strength and theoretical alignment, a full discharge-charge cycle was conducted on a 2 Ah Li-ion battery at a constant current of 1 A. The RMS voltage (V_{RMS}) of secondary coil was tracked and segmented across different cycle regions to assess its alignment with known electrochemical and mechanical transitions. RMS voltage is selected as the sensing metric as it provides a stable, time-averaged representation of the induced signal that is less sensitive to phase shifts and transient noise.

If the V_{RMS} response matched theory, the measurement moved on to stress testing the battery at higher discharge rates. Since discharge rate (C-rate) is proportional to the constant load current, the battery discharge at a high discharge rate will deplete faster, resulting in larger internal stress and temperature change. These tests aimed to confirm whether MF signal variations were sensitive to thermal and current-induced stress.

The third phase involved testing the sensing mechanism for a larger cell. This includes the use of an aged 20 Ah battery with a 1s2p configuration and reduced capacity. Discharge tests were conducted at low rates (0.05 C and 0.1 C) to observe the MF sensor's performance under a different geometry and degradation state.

In the next phase, a piezoresistive force sensor was introduced between the two parallel battery cells. This allowed for comparative analysis of MF and mechanical strain sensing. Signal-to-noise ratio (SNR) was calculated for both sensors. If the MF sensor showed superior SNR, the test progressed to a degradation trial. Here, the battery was intentionally stressed using undervoltage and cold-soak conditions to evaluate whether the MF signal could reflect abnormal internal states linked to ageing or damage.

Finally, if the MF response showed health-related degradation, the sensor was qualified for both state and health monitoring. Otherwise, it was limited to state monitoring.

III. Experimental Setup

The experimental setup, as shown in Fig. 2 was implemented. All tests were conducted inside a thermal chamber set to an ambient temperature of 20 °C (Fig. 2a). The chamber was controlled by Inkbird (model: ITC-308), maintained a controlled environment with an accuracy of ±0.3 °C. Two K-type thermocouples were used: one attached to the cell's surface to measure its temperature and the other inside the chamber but not connected to the cell. The test batteries were a 2 Ah Li-ion pouch cell (single cell) for the first test and a 20 Ah Li-ion module (1s2p configuration) for the second test. Both cells had a nominal voltage of 3.7 V, using Li-ion polymer chemistry with lithium cobalt as the cathode and graphite as the anode. The 2 Ah cell was new, while the 20 Ah module consisted of two pouch cells in parallel that had been used and intentionally aged.

Magnetic excitation and sensing were made using a pair of circular coils with 250 turns and 40mm diameter, as shown in Fig. 2b. They were wound on a plastic former and kept at a fixed distance with the battery placed in between the coils. The flat side of the battery was positioned in parallel to the MF lines. The primary coil was driven by a function generator at 10V peak, 94 kHz and the oscilloscope connected to both the primary and secondary coils records the signal. The secondary coil output was passed through an RMS to DC converter circuit to produce a DC voltage proportional to the RMS induced voltage. For experimental validation, external coils are used in

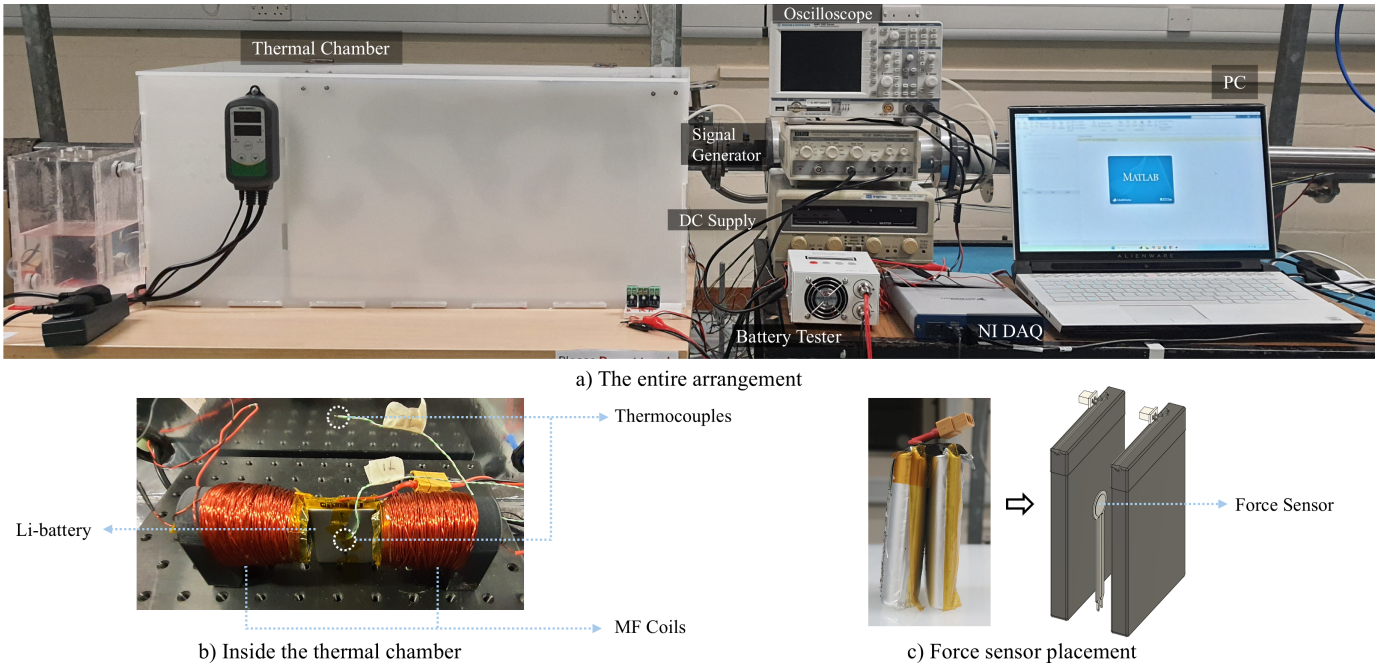


Fig. 2. Experimental setup for MF and Force sensor arrangements.

this setup but for real world application, planar or integrated coils can be utilized for compactness.

For the latter part of the experiment, as shown in Fig. 2c, a piezoresistive thin film force sensor (model: RP-C10-LT) was used to monitor stress or strain across the 20 Ah battery alongside the MF sensor. These sensors are not affected by electromagnetic interference and thus ideal for this purpose. They were sandwiched between the two cells and clamped externally. Consequently, any swelling or contraction of the cells would cause a change in resistance.

The batteries underwent cycling using a programmable battery tester (model EBC-A20). This tester allows for various cycle tests, adjustable charging and discharging rates and real-time monitoring of terminal voltage and current. A National Instruments data acquisition device (NI-USB6342) logged the analog outputs of the MF sensor, force sensor and thermocouple with a sampling frequency of 200 kHz. The battery tester also provided logs of current, voltage and capacity. Two test categories were conducted to observe the MF sensor's response: First, a healthy and low-rated battery was cycled at different rates to study the MF sensor's behaviour. Second, a degraded cell was cycled and the MF sensor's and force sensor's responses compared. The cells were further deteriorated to observe the MF sensor's response to battery health degradation.

IV. Results and Discussions

A. Low-Rated Battery Cycle Test

The 2 Ah battery underwent a standard constant-current and constant-voltage (CC-CV) discharge-charge cycle at a rate of 0.5 C (1 A) with 10-minute rest at the end of each cycle. The CC discharge involves discharging the cell with a constant load current of 1 A until the battery voltage drops to 3 V. The CV charging phase involves charging the battery with a fixed supply of 4.2 V. As the battery charges, it reaches the nominal 4.2 V and thus current entring the battery starts to drop. Charging is stopped when the current reaches 0.1 A (10% of 1 A).

Fig. 3 shows the corresponding voltage-current curve alongside the MF sensor's V_{RMS} change and its impact on surface and external temperature over 5.5 hours of battery cycling. The cycle was divided into eight phases with respect to various phenomena.

As shown in different Phases in Fig. 3, Phase I is the start of CC discharge, voltage sharply drops from 4.1 V to 3.8 V and then continues to steadily decrease. Meanwhile, the surface temperature rises sharply while the external temperature remains constant at 20 °C within the thermal chamber. The MF response is characterised by a decrease in the V_{RMS} value. This behavior is attributed to rapid Li-ion intercalation, reducing magnetic susceptibility [13]. Mechanically, the sudden discharge current causes a relaxation [14].

In phase II, the CC discharge continues and the V_{RMS} increases along the path. During discharge, the battery's volume decreases, causing a net strain that increases its magnetic susceptibility [15] [16]. This explains the MF sensor's behaviour. A 5°C temperature difference between the surface and chamber also highlights the induced mechanical strain on the battery. Phase III is a rest stage before charging begins, during which the V_{RMS} remains relatively constant. The surface temperature then starts to drop.

Phases IV-VII represent the discharging phase at CV. Phases IV and VI are explained by the rapid intercalation of lithium

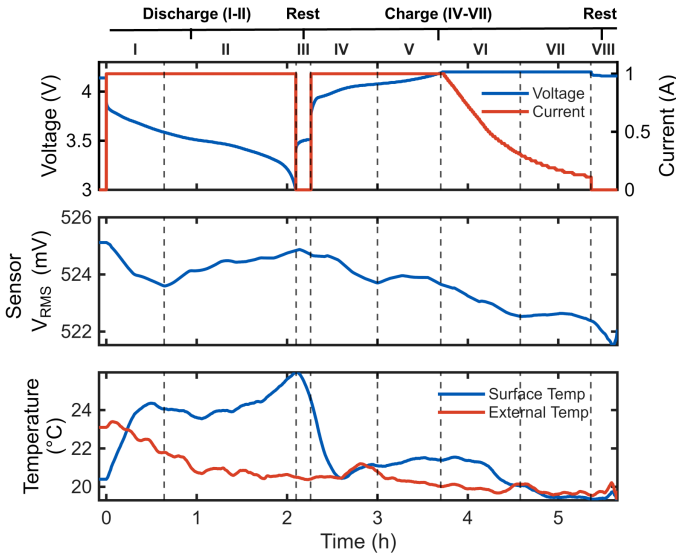


Fig. 3. Response of MF sensor and battery temperature (surface and external) with discharge-charge cycle.

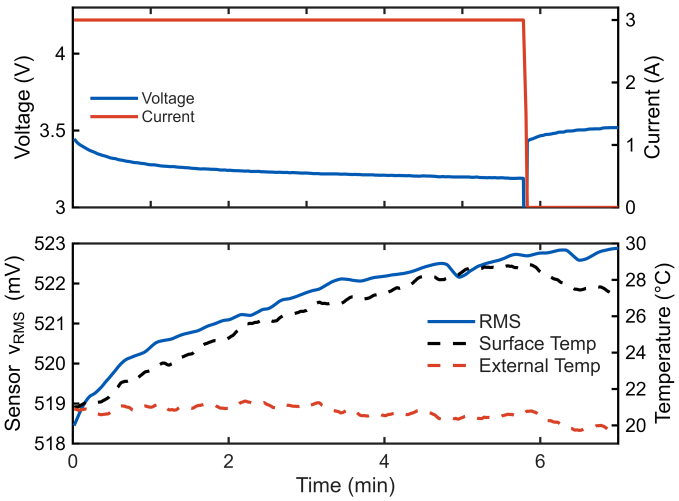


Fig. 4. Response of MF sensor and battery temperature at 1.5 C rate.

ions [17], causing volume expansion and resulting in a drop in V_{RMS} (opposite of Phase II). Phase V sees a steady surface temperature and constant intercalation and strain rates, leading to a flat current-voltage (MF) signal. Phase VII marks the end of charging with very slow lithium intercalation and a stable temperature, maintaining a V_{RMS} of 522.8 mV for most part of the duration and dropping to 522.4 mV close to the end. Finally, phase VIII is the rest phase after charging, showing a drastic drop in the V_{RMS} as the current drops to zero.

B. MF Sensor Response to High Discharge Rate

The 2 Ah battery was discharged at a higher rate (3 A, 1.5 C) to see the effect on MF sensing. Fig. 4 shows that the MF sensor's V_{RMS} and temperature rise rapidly during this cycle period. The cell starts near 4.1 V and is discharged at 3 A until the automatic cutoff at around 7 minutes due to the internal temperature limit. The V_{RMS} increases significantly with time, while the cell's surface temperature rises about 10 °C above ambient. The battery management system disconnected the cell due to temperature limit crossing, and thus battery voltage could not reach the 3 V mark. Within this short span of discharge time, there was a significant rise in V_{RMS}, increasing by 4 mV, as compared to the previous low-rated (1 A, 0.5 C) test. During the previous test, the V_{RMS} increased by only 2 mV over 2.5 hours. These results confirm that higher current induces greater internal stress or strain (and heating), which the MF sensor and thermocouple both capture.

C. Degraded Battery Cell Test

The 20 Ah (nominal) module, which had deteriorated to an actual capacity of 5 Ah, was tested. This cell is physically larger and stiffer than the 2 Ah pouch cell and, due to heavy ageing, exhibits higher internal resistance and increased heat generation even at low currents. It was tested at low C-rates (0.05 C and 0.1 C), and a piezoresistive force sensor was used alongside the MF sensor. The sensor placement is shown in Fig. 2c.

Fig. 5 depicts the response of MF and the force sensor as the battery was discharged from 3.4 V to 3.34 V. All responses showed a rising pattern as the battery was discharged. The MF sensor response was plotted as the change in V_{RMS} with respect to the initial V_{RMS}. This indicates that throughout this discharging region, the V_{RMS} change observed at 0.1 C was consistently greater than the change measured at 0.05 C. For the force sensor response, values rose from 3300 Ω to 3360 Ω for a 0.1 C rate and from 3350 Ω to 3420 Ω for a 0.05 C rate. The MF sensor's response aligns with the battery state, as a degraded cell discharged at a higher rate is expected to produce more stress or strain. The force sensor's data may not provide a comprehensive picture of the battery due to its single-point placement and measurement of only external deformation. In contrast, the MF sensor encompasses the entire battery cell and provides a complete view of the cells within its region. The results are compared in Table II. Another observation is that the V_{RMS} sensitivity is markedly higher for the larger, aged cell. During discharge, the 2 Ah cell exhibits a sensitivity of 1.7 mV/V, whereas the 20 Ah cell shows 66.7 mV/V, corresponding to nearly a 40-fold increase in sensitivity.

The signal-to-noise ratio (SNR) of the MF sensing channel and the piezoresistive force sensing channel was evaluated under identical experimental conditions, including the same thermal environment, data acquisition system, sampling parameters, and test protocol. Although the two sensors rely on different transduction mechanisms, both signals were ultimately measured as voltages by the same DAQ, with the force sensor resistance inferred through a voltage divider circuit. Therefore, the reported SNR values represent a comparison of the overall measurement-channel robustness rather than an intrinsic comparison of sensing principles. Within this experimental framework, the MF sensing channel exhibited a higher relative SNR of +11.78 dB than the force sensing

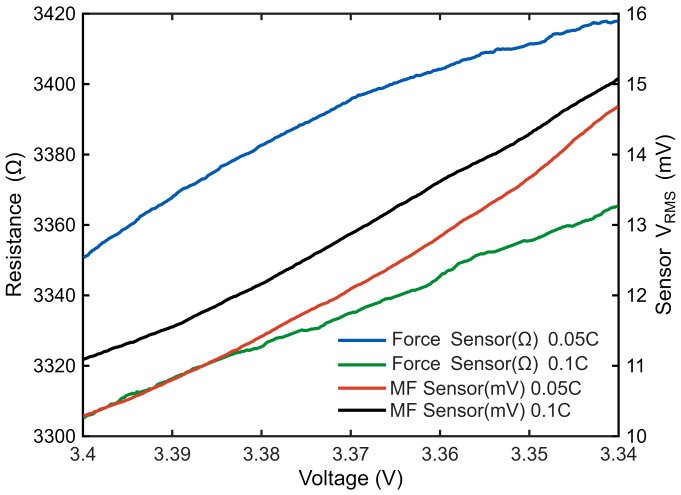


Fig. 5. Comparative overview of the battery discharge achieved by the MF and force sensors.

channel (-2.93 dB). To test the MF sensor's response to battery health degradation, a 20 Ah battery was completely discharged and placed below 0 °C for approximately two weeks. Upon testing, the battery capacity decreased from 5000 mAh to 3300 mAh and exhibited signs of swelling. The V_{RMS} of the MF sensor exhibited an increase of 7 mV, corresponding to a sensitivity of about 117 mV/V (previously this was 66.7 mv/V). The force sensor's sensitivty dropped to 66.7 Ω/V from 917 Ω/V over the same range.

TABLE II
COMPARISON OF MF AND FORCE SENSORS' RESPONSE TO BATTERY CYCLING TEST

Test Type	MF Sensor	Force Sensor
0.05 C Test (range)	10.2-13.2 mV	3350- 3420 Ω
0.1 C Test (range)	11-15 mV	3300- 3360 Ω
Avg. SNR (channel)	11.78 dB	-2.93 dB
Induced Damage Test (sensitivity)	117 mv/V	66.7 Ω/V

V. CONCLUSION

This study demonstrates that MF sensing offers a practical, cost-effective and non-invasive approach for assessing the internal condition and health of lithium-ion batteries. An experimental framework was designed by observing the changes in the root mean square induced voltage of the secondary coil of a two-inductive-coil system. The primary coil was energised with a 10 V peak, 94 kHz signal. The MF sensor was tested for a small (2 Ah) cell and its variations were checked along a full discharge-charge cycle. The methodology was further tested at different discharge rates with a larger multi-cell (20 Ah) and compared against a conventional thin-film force sensor. The results demonstrated that this proposed MF sensing offers non-invasive monitoring of lithium-ion states and health and can monitor effectively with a better signal-to-noise ratio than force sensors. Future work will include the improvement of the overall system for a multi-sensor system, the monitoring of the state of charge and state of health and the training of sensor data on a smart system.

REFERENCES

[1] S. Alagarsamy, P. Vishnuram, Y. Shanmugam, T. Thentral Tm, R. Gono, M. Gono, and R. Narayanamoorthi, "Advancements and Challenges in Lithium-Ion Battery Lifecycle Management Toward a Sustainable Circular Economy for Electric Vehicles," *IEEE Open Journal of Power Electronics*, vol. 6, pp. 1491–1533, 2025.

[2] F. I. Khan, M. M. Hossain, and G. Lu, "Sensing-based monitoring systems for electric vehicle battery – A review," *Measurement: Energy*, vol. 6, p. 100050, 6 2025.

[3] K. Yang, L. Zhang, Z. Zhang, H. Yu, W. Wang, M. Ouyang, C. Zhang, Q. Sun, X. Yan, S. Yang, and X. Liu, "Battery State of Health Estimate Strategies: From Data Analysis to End-Cloud Collaborative Framework," *Batteries 2023, Vol. 9, Page 351*, vol. 9, p. 351, 7 2023.

[4] S. Kocsis Szürke, M. Szabó, S. Szalai, and S. Fischer, "Deformation Analysis of Different Lithium Battery Designs Using the DIC Technique," *Energies 2024, Vol. 17, Page 323*, vol. 17, p. 323, 1 2024.

[5] Y. Zhang, K. Gao, T. Ma, H. Wang, and Y. F. Li, "Intelligent recognition of structural health state of EV lithium-ion Battery using transfer learning based on X-ray computed tomography," *Reliability Engineering & System Safety*, vol. 251, p. 110374, 11 2024.

[6] I. Escher, M. Hahn, G. A. Ferrero, and P. Adelhelm, "A Practical Guide for Using Electrochemical Dilatometry as Operando Tool in Battery and Supercapacitor Research," *Energy Technology*, vol. 10, p. 2101120, 5 2022.

[7] L. Albero Blanquer, F. Marchini, J. R. Seitz, N. Daher, F. Bétermier, J. Huang, C. Gervillié, and J. M. Tarascon, "Optical sensors for operando stress monitoring in lithium-based batteries containing solid-state or liquid electrolytes," *Nature Communications 2022 13:1*, vol. 13, pp. 1153–, 3 2022.

[8] L. Gold, T. Bach, W. Virsik, A. Schmitt, J. Müller, T. E. Staab, and G. Sextl, "Probing lithium-ion batteries' state-of-charge using ultrasonic transmission – Concept and laboratory testing," *Journal of Power Sources*, vol. 343, pp. 536–544, 3 2017.

[9] N. Khare, P. Singh, and J. K. Vassiliou, "A novel magnetic field probing technique for determining state of health of sealed lead-acid batteries," *Journal of Power Sources*, vol. 218, pp. 462–473, 11 2012.

[10] P. Singh, N. Khare, and P. K. Chaturvedi, "Li-ion battery ageing model parameter: SEI layer analysis using magnetic field probing," *Engineering Science and Technology, an International Journal*, vol. 21, pp. 35–42, 2 2018.

[11] C. M. Costa, K. J. Merazzo, R. Gonçalves, C. Amos, and S. Lanceros-Méndez, "Magnetically active lithium-ion batteries towards battery performance improvement," *iScience*, vol. 24, p. 102691, 6 2021.

[12] K. Shen, X. Xu, and Y. Tang, "Recent progress of magnetic field application in lithium-based batteries," *Nano Energy*, vol. 92, p. 106703, 2 2022.

[13] A. J. Ilott, M. Mohammadi, C. M. Schauerman, M. J. Ganter, and A. Jerschow, "Rechargeable lithium-ion cell state of charge and defect detection by in-situ inside-out magnetic resonance imaging," *Nature Communications 2018 9:1*, vol. 9, 5 2018.

[14] J. Peng, X. Zhou, S. Jia, Y. Jin, S. Xu, and J. Chen, "High precision strain monitoring for lithium ion batteries based on fiber Bragg grating sensors," *Journal of Power Sources*, vol. 433, p. 226692, 9 2019.

[15] A. J. Louli, L. D. Ellis, and J. R. Dahn, "Operando Pressure Measurements Reveal Solid Electrolyte Interphase Growth to Rank Li-Ion Cell Performance," *Joule*, vol. 3, pp. 745–761, 3 2019.

[16] U. Miniotaite, O. K. Forslund, E. Nocerino, F. Elson, R. Palm, N. Matsubara, Y. Ge, R. Khasanov, G. Kobayashi, Y. Sassa, J. Weissenrieder, V. Pomjakushin, D. Andreica, J. Sugiyama, and M. Månsson, "Magnetic Properties of Multifunctional 7LiFePO4 under Hydrostatic Pressure," *Journal of Physics: Conference Series*, vol. 2462, p. 012049, 3 2023.

[17] X. Wang, Y. Sone, and S. Kuwajima, "In Situ Investigation of the Volume Change in Li-ion Cell with Charging and Discharging: Satellite Power Applications," *Journal of The Electrochemical Society*, vol. 151, p. A273, 1 2004.